Macromolecules
ARTICLE

*Macromolecules* **2010**, *43*, 299–305 **299**
DOI: 10.1021/ma9018069

# Concentration Effect on the Oriented Microstructure in Tensile Drawn Polyfluorene−Polyethylene Blend

**Matti Knaapila,*,† Helen L. Vaughan,*,‡ Thomas P. A. Hase,§ Rachel C. Evans,∥,⊥ Roman Stepanyan,¶ Mika Torkkeli,# Hugh D. Burrows,∥ Ullrich Scherf,▽ and Andrew P. Monkman‡**

†*Department of Physics, Institute for Energy Technology, NO-2027 Kjeller, Norway,* ‡*Department of Physics, University of Durham, Durham DH1 3LN, England,* §*Department of Physics, University of Warwick, Coventry CV4 7AL, England,* ∥*Departamento de Química, Universidade de Coimbra, PO-3004-535 Coimbra, Portugal,* ⊥*Departamento de Física, CICECO, Universidade de Aveiro, PO-3810-193 Aveiro, Portugal,* ¶*Materials Science Centre, DSM Research, NL-6160 MD Geleen, The Netherlands,* #*Department of Physics, FI-00014 University of Helsinki, Finland, and* ▽*Fachbereich Chemie, Bergische Universität Wuppertal, DE-42097 Wuppertal, Germany*

*Received August 12, 2009; Revised Manuscript Received November 10, 2009*

ABSTRACT: We report on the segregation and microstructure of poly[9,9-bis(2-ethylhexyl)-fluorene] (PF2/6) blended in polyethylene (PE) aligned by tensile drawing at elevated temperature. X-ray diffraction and photoluminescence data indicate that when the PF2/6 fraction is high (7−15 wt %), PF2/6 assembles in uniaxially aligned crystallites (the coherence length ∼32 nm) segregated within the PE matrix. The full-width-half-maximum of the PF2/6 crystallite orientation distribution about the stretching direction is ≤10°. No significant macrophase separation is observed with AFM or optical and fluorescence microscopy. When the PF2/6 fraction is low (0.25 wt %), aligned PF2/6 forms a frozen-in nematic-like phase. The aligned polymers remain closely located but their coherence length is significantly decreased (∼8 nm), which is attributed to the decreased crystallite size. This behavior differs from that of poly(phenylene-vinylene) type polymers and the difference is rationalized by compatibility and entanglement arguments.

## Introduction

Phase behavior and structure formation are essential factors in the physics and materials science of $\pi$-conjugated polymers[1] such as polyfluorenes (PFs).[2] The majority of research efforts into the structure of PFs have been directed toward chemical and intramolecular structures but attention is increasingly devoted to intermolecular assemblies (or structural levels) as well as nano- and microstructures.[3] The structural levels beyond molecules are conventionally prepared by bottom-up methods such as block copolymer synthesis[4] or by top-down methods such as microporous templates.[5] While phase separation of block copolymers is constrained by chemical bonds, blending two or more polymers allows phase variations from complete miscibility to macrophase separation. With the selective cross-linking and polymer removal, the blend can also act as a template for a porous polyfluorene structure.[6] Blending allows, moreover, a facile combination of electron-donating and electron-accepting materials. This has significant implications in areas such as polymer photovoltaics[7] where the former one is absorbing sunlight and the latter one collecting electrons.

Examples of PF blends include poly(9,9-dioctylfluorene) (PF8) and polystyrene (PS),[8] PF8 and polyethylene (PE),[9] PF8 and polymethylmethacrylate (PMMA),[10,11] poly(9,9-dioctylfluorene-*co*-benzothiadiazole) (F8BT) and poly[9,9-dioctylfluorene-*co*-*N*,*N*′-bis(4-butylphenyl)-*N*,*N*′-diphenyl-1,4-phenylenediamine] (PFB)[12] and PF8 and F8BT[13] as well as diverse PF copolymers.[14] Further structural levels are obtained when these blends are modified with top-down methods such as electrospinning.[11,15] Alignment of PF blends, in turn, controls macroscopic anisotropy within the blend as reflected by anisotropic optical characteristics. An interesting example is provided by King et al.[16] who demonstrated how an oriented blend of poly[9,9-bis-(2-ethylhexyl)-fluorene] (PF2/6) and PE can be used as a tool to track the orientation of PF singlet and triplet transition dipole moments. Yet structural and phase behavioral studies of aligned PF blends remain sparse.

Heeger and co-workers combined blending with alignment and studied structure formation of $\pi$-conjugated poly[2-butyl-5-(2′-ethylhexyl)-1,4-phenylene-vinylene] (or BuEH-PPV) blended in high molecular weight PE.[17] These authors raised the BuEH-PPV fraction up to 30 wt %, aligned these samples by drawing and studied them by X-ray diffraction (XRD). They found that 30 wt % blend of BuEH-PPV forms a uniform mixture of crystallites in nonaligned samples but a uniform mixture of individual chains in aligned samples, a structure denoted as an interstitial microfiber. It is not known whether this microfiber phenomena plays a role in PF blends.

In this paper, we report on a microstructure of aligned PF2/6 blended in PE. The paper has two objectives. First, it aims to provide a structural counterpart to the optical work of King et al.[16] who used low PF fraction ( < 0.7 wt %). Second, it aims to provide the materials counterpart to the work of Heeger et al.[17] who used PPV and high guest fraction. To cover the concentration regimes of both studies,[16,17] the PF2/6 fraction was varied between 0.25 and 15 wt %. The materials selection was also motivated by the fact that PF2/6 represents a well-studied structural archetype for PF alignment.[18,19]

We distinguish two cases based on XRD. If the PF2/6 fraction is high (7−15 wt %) the blend is found to be a macroscopically

*To whom correspondence should be addressed. E-mail: (M.K.) matti.knaapila@ife.no; (H.L.V.) h.l.vaughan@durham.ac.uk.



Published on Web 12/08/2009

**Chart 1. Chemical Structure of PF2/6 Polymer**

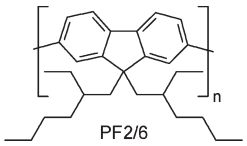


uniform mixture of aligned PE and PF2/6 (with coherence length ~30 nm) crystallites; if the PF2/6 fraction is low (0.25 wt %), the blend behaves similarly but the coherence length of PF2/6 is significantly decreased (~8 nm). Apart from large amounts of self-absorption in the higher concentration samples, the photoluminescence (PL) data are essentially the same and correspond to that of pure solid PF2/6, which indicates that the PF2/6 chains are located in the vicinity of each other. Therefore, the reduction in coherence length is understood to involve a decrease in crystallite size. Unlike the case of BuEH-PPV,[17] the crystallites are present in a very well aligned sample (full width at half-maximum (fwhm) of the mosaic distribution is $\leq 10°$). This difference between the PPV type polymer and PF is explained in terms of compatibility, entanglement, and backbone stiffness. This study provides an insight on crystallite segregation in aligned PF:PE blends. As similar PE blending and alignment procedures have been used for a diverse set of semirigid[20−22] and rigid[23] $\pi$-conjugated polymers that have not, however, been studied by fiber XRD, the results presented here may have implications beyond the studied polymer.

## Experimental Section

**Materials.** PF2/6, with the number average molecular weight ($M_n$) = 262 kg/mol, weight average molecular weight ($M_w$) = 466 kg/mol (Chart 1) was prepared as described previously.[2,18] Spectrophotometric grade PE ($M_n \approx 80$ kg/mol) with melting point of 130−145 °C was supplied by Sigma-Aldrich (product number 269352). Blending and alignment were performed at elevated temperatures (above the glass transitions of both polymers) as described in refs 16 and 22. This procedure involved dissolving PE and PF2/6 into *o*-xylene at 120 °C. Once a perfectly clear PE solution was obtained, the solution was cooled to 90 °C. After this, an *o*-xylene solution of PF2/6 was added to the PE solution and stirred thoroughly. This solution was allowed to cool slowly in thin films that were tensile stretched to up to 30 times their original length using the hot pin method. In this method, strips of the blend were held over the edge of a thin metal bar that was heated until the PE film began to melt. At this point, the films were stretched slowly above the bar. The thickness of the film was ~1 mm before stretching and ~100 $\mu$m after stretching. For optical and X-ray measurements the films were cut and attached to a quartz slide. In this configuration, corresponding to the classification of Heffelfinger and Burton,[24] the $x$ axis is defined as the surface normal whereas $y$ and $z$ axes are parallel to the surface so that the $z$ axis points to the stretching direction and is denoted as the fiber axis (c.f., Figure 1). The terms meridional and equatorial refer to the $z$ axis and ($xy$0) plane, respectively. All subsequent characterization was carried out at room temperature.

**Instrumentation and Methods.** Optical microscopy was performed using a Nikon 115 optical microscope equipped with crossed polarizers.

Atomic force microscopy (AFM) was carried out using a Surface Imaging Systems STM/AFM in noncontact mode. The system was mounted on a PicoStation placed on a Halcyonics MOD-1 M Plus active vibration isolation system.

Fluorescence microscopy (FM) was carried out using an Olympus BX51 M microscope in epifluorescence mode (excitation and detection from above the film) and used the filter set type U-MNU2 (360−370 nm excitation and 400 nm dichroic mirror), which allowed visible emission wavelengths

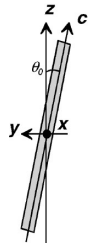


**Figure 1.** An illustration of the alignment geometry. The vectors **z** and **c** represent the overall alignment direction and, more locally, the backbone of a rigid molecule, respectively. The angle $\theta_0$ represents the angle between the alignment direction (**z**) and the backbone of the polymer (**c**). In a XRD $\phi$-scan, the sample is rotated about $x$ axis.

greater than 405 nm to be observed. Samples were illuminated with a UV-mercury lamp (100 W Ushio Olympus). Images were recorded with a digital camera (Olympus DP70).

Initial XRD measurements were carried out in glancing angle geometry at the W1.1 (ROEWI) beamline at HASYLAB at DESY in Hamburg (Germany). The beam (10.5 keV, 0.1 mm × 0.4 mm (vertical × horizontal)) was monochromatized by a double crystal Si(111) monochromator and focused onto the sample. Separate XRD patterns were measured with the incident beam along the $z$ and $y$ axes using an image plate (Molecular Dynamics). For normalization, the incident flux was measured with an ionization chamber. A helium atmosphere was employed to reduce background and suppress radiation damage.

The XRD patterns as a function of azimuth angle ($\phi$), so-called $\phi$-scans, were carried out at the XMaS beamline at the ESRF in Grenoble, France. The beam (11 keV, 0.2 mm × 1 mm (vert × hor)) was monochromated using a double Si(111) crystal and focused on the sample. The experiments were performed in the glancing angle geometry by varying $\phi$ and keeping the $x$ axis perpendicular to the incoming beam. The zero of the rotation angle, $\phi = 0°$, is defined when the scattering plane is coincident with the $z$ axis. For this scan, the surface of the sample was aligned flat using a reflected laser beam. The scattering data were measured using a MarCCD165 detector. This procedure and subsequent data analyses were adapted from ref 25.

Optical absorption measurements were performed using a Perkin-Elmer Lambda 19 spectrometer. PL measurements were performed using a Jobin-Yvon Fluoromax fluorimeter equipped with Glan-Thompson polarizers. The excitation wavelength was 360 nm for measurements without polarizers and 385 nm for measurements with polarizers.

## Results and Discussion

Preparation of oriented films of PF2/6:PE blend followed the procedure described in the previous report of King et al.[16] However, while that work dealt with low PF2/6 fraction ($< 0.7$ wt %), the present work considers both low (0.25 wt %) and high (7−15 wt %) PF2/6 fractions. The question is whether macrophase separation occurs at the high PF2/6 fraction limit. Serious macrophase separation is expected to cause patchy surface morphology similar to those reported for PE blends in ref 26.

Figure 2 shows an optical micrograph of the PF2/6:PE blend with the mixing ratio (PF2/6 to PE) of 15:85. The film appears uniform with distinctive ridges and furrows along the stretching direction (Figure 2a). Furthermore, the films are birefringent as expected for aligned polymer chains (Figure 2b). No evidence for macrophase separation is seen but this possibility cannot be fully excluded. Figure 3 shows the characteristic AFM topography of the same film. Visually observed ridges and furrows scale down to submicrometer scale and follow preferential texture without apparent imperfections of gross macrophase separation like in ref 26.

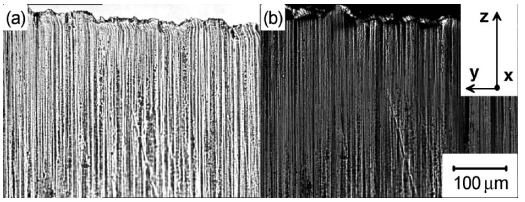


**Figure 2.** Optical micrographs of aligned PF2/6:PE blend with the mixing ratio of 15:85 as measured in transmission geometry without (a) and with (b) crossed polarizers. The marked axes correspond to those shown in Figure 1.

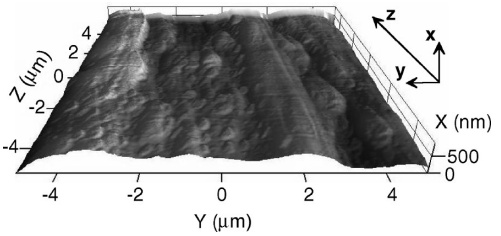


**Figure 3.** Surface morphology of aligned PF2/6:PE blend with the mixing ratio of 15:85 as measured by AFM. The illustrated area is 10 $\mu$m × 10 $\mu$m wide and the highest peak 0.5 $\mu$m high.

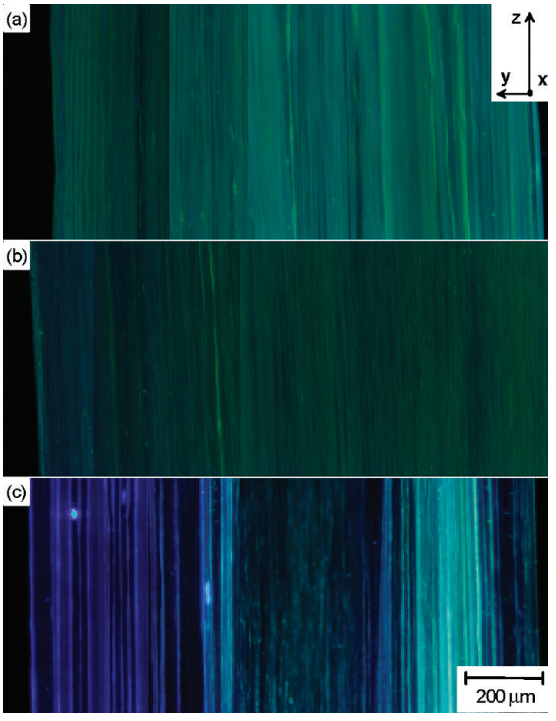


**Figure 4.** Fluorescence microscopy images of aligned PF2/6:PE blend with the mixing ratio of 15:85 (a), 7:93 (b), and 0.25:99.75 (c). The figure shows blue or pale turquoise fluorescent stripes from the PF2/6 and dark stripes from the PE rich regions.

Figure 4 shows the FM images of PE:PF2/6 blends with the mixing ratios of 15:85, 7:93 and 0.25:99.75 obtained for excitation at 360−370 nm. When the PF2/6 fraction is high (7−15 wt %), the blend is found to be a macroscopically uniform mixture of PE and PF2/6 down to the micrometer scale, observed as homogenously aligned fluorescent strandlike structures (Figure 4a,b). Self-absorption of PF2/6 is expected to mask blue PF fluorescence on the film surface such that it appears as pale blue or turquoise, instead of blue, in the FM image. When the PF2/6 fraction is low (0.25 wt %), fluorescent blue stripe-like structures are observed with intermittent darker elongated

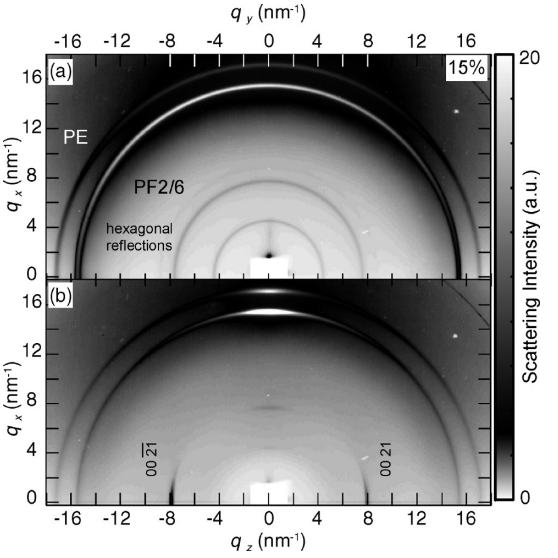


**Figure 5.** XRD images of aligned PF2/6:PE blend with the mixing ratio of 15:85. (a) ($xy$0) plane, $\phi$ = 0° and (b) ($x$0$z$) plane, $\phi$ = 90°.

domains orientated parallel to the stretching direction (Figure 4c). The dark areas are attributed to PE rich regions, as a result of putative phase separation on the 10−50 $\mu$m scale. As both the excitation and fluorescence are measured from above the film, the dark areas cannot be attributed to the thickness variation in the film. Thus, while PF2/6 seems evenly distributed at the high concentration limit, possible macrophase separation is observed at the low concentration limit. However, even spatially uniform fluorescence of the PF2/6:PE film does not indicate that the polymers are mixed at the molecular scale but merely on the micrometer scale, as shown elsewhere, for instance for poly[2-methoxy-5-(2′-ethylhexyloxy)-1,4-phenylene-vinylene] (MEH-PPV) blended with PS.[27] On the other hand the fluorescence of pure PF is not uniform on submicrometer scale.[28] Also, the images may not give quantitative results of the local composition. To probe local structure and any kind of microphase separation, the films were also studied by XRD.

Figure 5 shows the XRD patterns of the PF2/6:PE blend with the mixing ratio of 15:85. The sample was measured with the X-ray beam parallel to both the $z$ axis (Figure 5a) and to the $y$ axis (Figure 5b) directions. The data shows a set of Bragg reflections clearly implying crystalline or semicrystalline structure. The low ($q \leq 10$ nm$^{-1}$) and high angle ($q \geq 10$ nm$^{-1}$) reflections are identified as the main reflections of pure PF2/6[29,30] and pure PE[31] indicating the co-existence of the corresponding crystallites. Unsurprisingly, the data are dominated by the reflections of the PE matrix while those of PF2/6 are weaker. Only reflections of pure compounds are observed, which indicate that PF2/6 coexists as separate crystallites within PE crystallites and not as separate chains within PE unit cells. The clear distinction between equatorial rings and meridional peaks indicates a fiberlike structure with high uniaxial (along $z$ axis) alignment without surface preference, an observation that is consistent with a one-dimensional alignment procedure. Thus, the blend with the mixing ratio of 15:85 is expected to contain a mosaic of uniaxially aligned PF2/6 crystallites within uniaxially aligned PE crystallites. The data of the blend with the mixing ratio of 7:93 (not shown) are essentially similar.

Figure 6 plots the XRD patterns of the PF2/6:PE blend with the mixing ratio of 0.25:99.75. As expected, the data are dominated by PE features akin to those shown in Figure 5. In contrast, the data differ with reference to the PF2/6 reflections. While the blend with the mixing ratio of 15:85 reveals sharp equatorial rings (Figure 5a), the blend with the ratio of 0.25:99.75 shows only

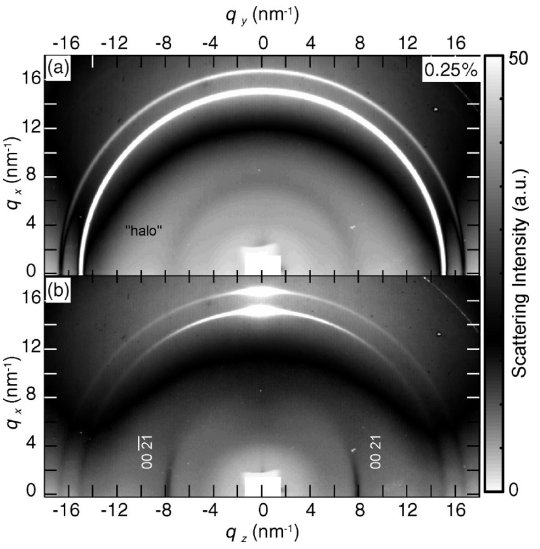


**Figure 6.** XRD images of aligned PF2/6:PE blend with the mixing ratio of 0.25:99.75. (a) ($xy0$) plane, $\phi = 0°$ and (b) ($x0z$) plane, $\phi = 90°$.

a shallow equatorial halo (Figure 6a). Furthermore, the meridional 005[29] (or 00 21[30]) peaks are considerably weaker (Figure 6b). There are two alternative explanations. First, there can be a different microstructure as compared with the blend with the higher mixing ratio. Second, the material could be a similar mixture of crystallites but with a smaller fraction of PF2/6. The distinction between these alternatives is not apparent, since the absence of sharp equatorial rings (corresponding to hexagonal packing) for lower mixing ratio can be attributed to the smaller materials fraction that suppresses the equatorial reflections. Therefore, attention should be placed on the peak widths of the PF2/6 reflections.

Figure 7 shows the relative intensities of the reflections of aligned PF2/6:PE blends with the mixing ratios of 15:85 and 0.25:99.75. Here, the 2D patterns are azimuthally averaged about out-of-plane and in-plane directions. The size of PE crystallites is 10.3 nm (~10 nm) for the 15:85 blend and 12.1 nm (~12 nm) for the 0.25:99.75 blend, as estimated from the equatorial 110 reflection. For both samples the degree of PE crystallinity is high and hardly any amorphous contribution is observed at 10−15 $nm^{-1}$. For the 15:85 blend, the estimated equatorial crystallite size for PF2/6 crystallites is 27.4 nm (~28 nm). Determination of equatorial peak width for the data of 0.25:99.75 sample proved to be unreliable but the comparison between the samples can be achieved by considering the meridional crystallite size based on the 00 21 reflection. The value obtained for the blend with mixing ratio of 15:85 is 31.8 nm (~32 nm). In contrast, the similarly obtained value for the blend with mixing ratio of 0.25:99.75 is only 7.9 nm (~8 nm). This significant difference indicates the presence of two different microstructures between the high and low blending ratios.

The former value is consistent with that found for the hexagonal structure in aligned PF2/6 fibres[32] and aligned films on rubbed polyimide.[25] This supports the hypothesis of segregated PF2/6 crystallites within the PE matrix with virtually constant crystallite size. The latter value for low ratios indicates considerable loss in lateral order and would correspond to the values found for PF2/6 in frozen-in nematic phase.[32] However, the comparison between observed loss in lateral order in the blend and the frozen-in nematic phase in the pure PF2/6 is not directly relevant. Pure PF2/6 assembles in hexagonal crystallites above the threshold molecular weight $M^*$ and assembles like frozen-in nematic structures below the threshold $M^*$ that is ~10 kg/mol at room temperature.[32] As the molecular weight of the present

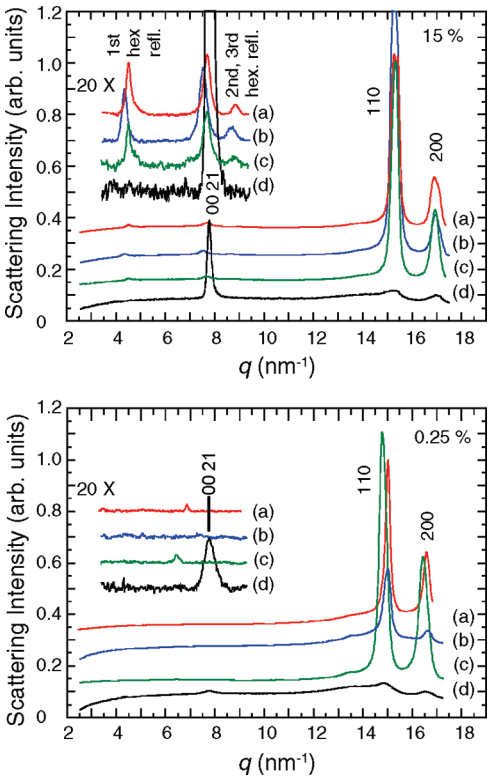


**Figure 7.** XRD patterns of aligned PF2/6:PE blend with the mixing ratio of 15:85 (upper panel) and 0.25:99.75 (lower panel). The 1D curves correspond to 10° azimuthal averages: X-ray beam nearly parallel to the $z$ axis - integral about the $x$ axis (a; red) and about the $y$ axis (b; blue). X-ray beam nearly parallel to the $y$ axis - integral about the $x$ axis (c; green) and about the $z$ axis (d; black). Inset shows a 20 times magnification of the area where the main reflections of crystalline pure PF2/6 should appear. The curves are offset for clarity.

samples was constant and well above the threshold (~300 kg/mol), the observed laterally less ordered phase cannot simply be explained as frozen-in nematic domains similar to those reported in ref 32. Moreover, as the preparation temperature was well-controlled and because all samples were heated above the glass transition of PF2/6 (which facilitates the crystallite growth), this difference in microphase structure cannot arise from different thermal history and must arise from the polymer itself.

The degree of alignment was assessed by the results of $\phi$-scans. This is achieved by rotating the films about the $x$ axis (see Figure 1) and integrating over the scattering intensities of the main reflections. Figure 8 shows examples of the obtained intensity distributions for the main reflections of high PF2/6 ratio blends. The fwhm ($=2.35\ \sigma$) values of these functions as calculated from the equatorial and meridional reflections of the blend with the mixing ratio of 15:85 are, respectively, $10.7 \pm 0.2°$ and $8.9 \pm 0.2°$. The corresponding fwhm as calculated from the meridional reflection of the blend with the mixing ratio 7:93 is $10.5 \pm 0.3°$. This indicates that the distributions are similar for the equatorial and meridional reflections in a single film and similar for two different concentrations.

The distributions of scattering intensities represent the alignment of rigid polymer sections in crystallites. As described in ref 25, this allows the estimation of the order parameter in 2D approximation as $s = \langle 2\cos^2\theta - 1\rangle = \int f(\theta)\cos 2\theta d\theta \simeq 1 - 2\theta_0^2$, where the magnitude of the angle $\theta_0$ (Figure 1) is estimated by two sigma (95% deviation of the mean). For blends with the mixing ratios of both 15:85 and 7:93, we estimate order parameters to be as high as ~0.95. The weak scattering features arising from the blend with low PF2/6 fraction did not allow us to perform satisfactory $\phi$-scans.

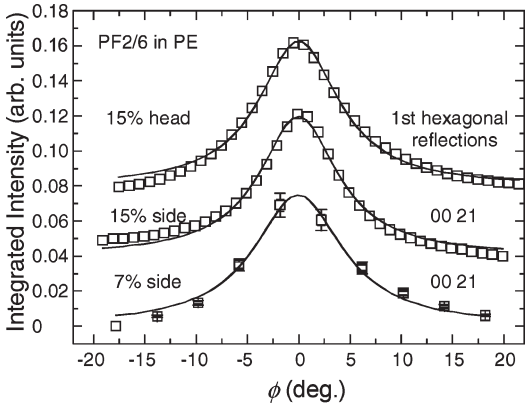


**Figure 8.** Integrated intensities of the first (equatorial) hexagonal reflections and meridional 00 21 reflections of aligned PF2/6:PE blends with mixing ratios of 15:85 and 7:93. The sample is rotated about the $x$ axis and $\phi$ is the angle between incident beam and $z$ axis. Percentages refer to the PF2/6 fraction. The solid lines are Lorentzian fits from which the width of the orientation is calculated.

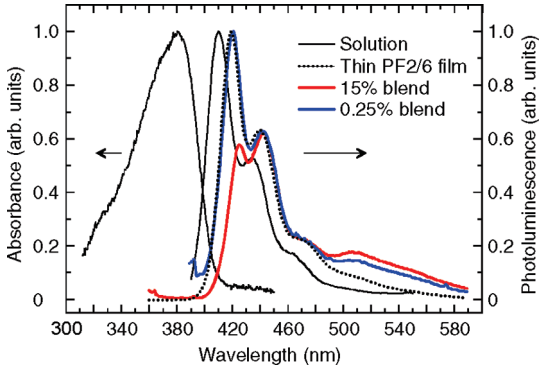


**Figure 9.** PL data of aligned films of PF2/6:PE blends with the mixing ratio of 15:85 (thick red line) and 0.25:99.75 (thick blue line). PL spectrum of pure PF2/6 film (black dotted line) and photoabsorption and PL spectra of 1% toluene solution (black solid lines) are shown for comparison. All PL spectra were taken with an excitation wavelength of 360 nm.

While XRD gives an indication of the crystalline order, fluorescence spectroscopy is a reflection of the structure at the molecular level.[33] Figure 9 plots PL spectra of the studied PE:PF2/6 blends with the mixing ratios of 15:85 and 0.25:99.75. The data of PF2/6 toluene solution and the data of a pure PF2/6 film spun from the toluene solution are shown for comparison. An absorption spectrum of the solution is shown in addition. The PL spectra of both blends are essentially the same, and correspond to that of pure polymer. This implies that the PF2/6 chains are located in the vicinity of each other in both samples. The high concentration blend shows significant self-absorption with increasing PF2/6 concentration, an effect that is seen in the FM images (Figure 4) and that is also seen for instance for PF8:PMMA blends.[11] The data are in agreement with the idea of microscopically segregated PF2/6 domains and not molecular level dissolution in high polymer fraction blends. The data from the low polymer fraction film (0.25:99.75) could be from single isolated chains that have been solvatachromatically red-shifted by 5 nm. However there is no way to rule out the possibility that there are also segregated domains. Though, from the lack of reabsorption in this film compared with the higher ratio film, it is hypothesized that the chains are further separated, which could be because the domains are significantly smaller or at a greater separation. Complete dilution and the corresponding complete separation of the chains down to the molecular level in the low

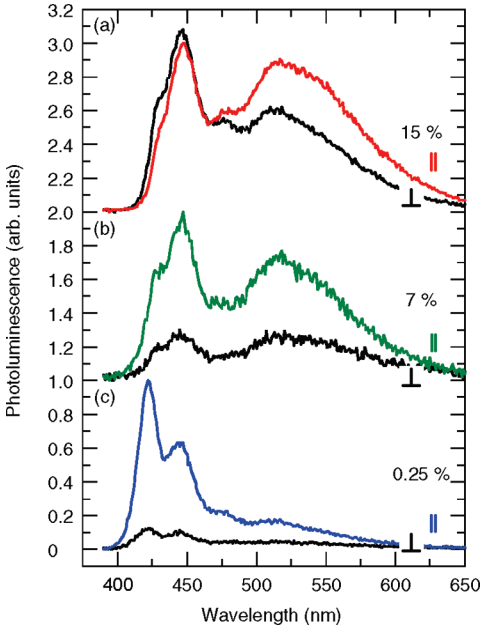


**Figure 10.** Polarized PL data of aligned films of PF2/6:PE blends with the mixing ratio of 15:85 (a), 7:93 (b), and 0.25:99.75 (c). The measurements have been carried out using polarized excitation with the polarization axis parallel to the z axis. The emission has been measured through the polarizer with the polarization axis parallel (red, green, and blue lines) and perpendicular to the $z$ axis (black lines). The excitation wavelength was 385 nm. The curves are staggered for clarity.

polymer fraction blend should be followed by an increase in the ratio of the intensity of the vibronic peaks (at 420 and 435 nm) as observed for PF solution (Figure 9).

Figure 10 shows the polarized PL data of aligned PF2/6:PE blends for the studied polymer fractions. PL polarization ratios of ~6:1, ~4:1, and ~1 are obtained for the mixing ratios 15:85, 7:93, and 0.25:99.75, respectively. The fluorescence polarization ratios can be used to estimate the overall orientation of the film. For example, an order parameter obtained from the PL of films with a mixing ratio 7:93 is $s_{PL} = (PL_{\parallel} - PL_{\perp})/(PL_{\parallel} + PL_{\perp}) \sim 0.6$, considerably lower than the value obtained by XRD (~0.95). The most plausible explanation is that the blends contain both highly aligned PF2/6 crystallites and some noncrystalline PF2/6 chains. These noncrystalline chains have less orientation than PF2/6 crystallites and when they all emit, the overall polarization ratio is lowered.

The green emission band at 510−520 nm, present in Figure 10, is indicative of fluorenone units forming a delocalized charge transfer state.[33] The isoemissive point between blue fluorene and green fluorenone emissions is located at around 500 nm. This band becomes relatively stronger with the strong self-absorption at high PF2/6 fraction. In this case, the excitons will be able to migrate easily to keto defects and form the charge transfer states that quench the emission of the PF2/6. The efficient energy transfer does not mean that the fluorenone population was inherently higher in the samples at higher polymer fraction.

From our results, the following model is proposed in Figure 11. A mosaic of aligned PF2/6 crystallites is observed for the high PF2/6 limit (7−15%) as shown in Figure 11a. The domain size estimated from a single meridional reflection is ~32 nm and their mosaic distribution about $z$ axis ≤10°. A mixture of PF2/6 bundles with the coherence length of ~8 nm is proposed for the low PF2/6 limit (0.25 wt %) as shown in Figure 11b. The coherence length of PE crystallites is similar (~10 nm) in both cases.

This picture is unable to clearly show the amorphous PE phase in which some of the single PF2/6 chains may be dissolved. The

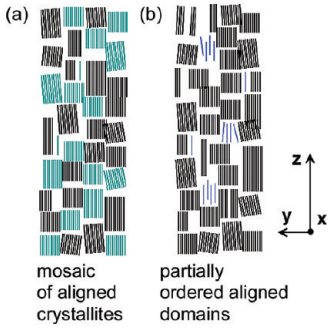


**Figure 11.** Schematics of aligned PF2/6:PE blends. (a) A mosaic of aligned crystallites at high PF2/6 fraction. The square shape of PF2/6 crystallites illustrates similar equatorial and meridional coherence length (~30 nm). (b) Segregated noncrystalline polymer domains at low PF2/6 fraction. A part of the chains are isolated. The turquoise refers to aligned crystalline PF2/6 and blue to aligned nematic-like PF2/6 domains (meridional coherence length of ~8 nm). Dark areas refer to aligned PE crystallites (size ~10 nm).

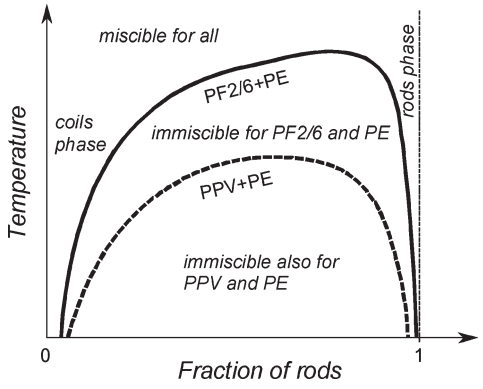


**Figure 12.** Expected phase diagram for PF2/6:PE and PPV:PE blends.

fraction of dissolved PF chains relative to the ordered material is expected to increase with decreasing PF content but the high PE crystallinity does not allow quantification of this effect. On the one hand, the amount of dissolved PF is expected to be small because the PL spectrum of a blend clearly deviates from the solution spectrum indicating a different solvatochromic effect in the film. There is also a detectable, ordered phase (but not a crystalline phase) in the 0.25 wt % blend that is different from an isotropic solution. On the other hand, the amount of dissolved PF could be large because the overall orientation from polarized fluorescence measurements is significantly lower than the crystallite orientation. The latter indicates a significant fraction of isolated poorly aligned PF chains presumably located within amorphous PE.

The questions as to why there is a difference between BuEH-PPV and PF2/6 and how the PF2/6 domains can be interpreted for the low PF2/6 fraction are as yet unanswered. Phenomenologically, we assume two structural differences between PF2/6 and PPV type polymers. The phase separation can be understood in terms of these differences. First, PF2/6 is less compatible with the PE matrix as it has a lower alkyl chain density than PPV, leading to a thinner interfacial layer between the host matrix and the guest polymer domains. Also, fewer bridges between crystallites (so-called tie molecules) are expected to be present resulting in lower forces exerted on the PF2/6 polymer domains as compared with PPV. This lower force might be enough to align them but too low to destroy the crystallites.

Second, PF2/6, while flexible, is stiffer than PPV and the implications of this can be understood in terms of mixtures of rodlike and flexible polymers. The phase diagram of rodlike and flexible polymers can be predicted in different ways (see ref 34) and its general form is shown in Figure 12. This diagram is also plausible for PF2/6 and PPV, which are both hairy-rodlike polymers, that is, rodlike polymers with flexible side chains. In this model, rodlike (guest conjugated polymer) and flexible (host PE) polymers are mixed. There is a reasonably large region of miscibility above the upper critical point (that may be too high to be observed in these experiments) and a large two-phase area (that corresponds to the immiscibility) that is located under the bell-shaped curve. The solid line is what we expect for PF2/6, whereas the dashed line sketches the PPV-PE binodal. The binodal is higher in PF2/6 because of the increased stiffness of PF2/6 and possible variation in Flory−Huggins type interaction.[35] Such details as nematic−nematic coexistence are omitted.

Due to the increased stiffness in PF2/6, which decreases the ability of the polymer to dissolve in PE, we expect this polymer to form significantly fewer entanglements with PE than the PPV type polymers. This is connected to the alignment process that involves annealing above the crystallization temperatures of the polymers (see Experimental section). At the high PF2/6 fraction limit (7−15 wt %), PF2/6 microphase separates and forms crystallites whose size corresponds to that observed in pure PF2/6. During tensile drawing the crystallites are aligned and possibly deformed but without strong entanglements they are not destroyed and they are still observed in drawn films (as seen in the XRD data).

In contrast, PPV molecules can form bridges (tie molecules) between crystallites.[17] During tensile drawing, many of the crystallites are destroyed and oriented molecules form "strings" within the PE matrix that retain an interaction between adjacent strings, resulting in a structure called an "interstitial microfiber".[17] A similar conclusion has been made for a PPV:PE blend by Weder et al.[21]

The interpretation is more complicated at the low PF2/6 fraction limit (0.25 wt %), where no crystallites are expected. This could be because they do not exist or they are smaller than in the higher concentration film.

The crystallites could be destroyed during the alignment, as in the case of PPV type polymer. This is, however, very unlikely as this would imply that the amount of entanglements increases with decreasing concentration, which is counterintuitive. Also the polymer and the sample preparation were identical to that employed in the high PF2/6 fraction case where no crystallite destruction is seen.

A second, more likely, scenario is that the crystallites are too small to give sharp Bragg reflections but instead cause broad interference maxima (as seen in Figure 6). Generally speaking, peak broadening of this kind can arise from decreased crystallite (ordered domain) size, paracrystallinity, microstrain, or instrumental smearing. Here, instrumental broadening is negligible and moreover identical in the results from all our samples. PF2/6 is paracrystalline by nature[32] and microstrains can reasonably be thought to exist in tensile drawn samples; however, these effects are assumed to be small and similar in identically manufactured samples. Ruling out these other causes of the peak broadening means the decrease in crystallite size and not the destruction of crystallites remains the most plausible explanation. This phenomenon of small crystallites is likely to be linked to the kinetics of crystallization, which is however beyond our present, phenomenological discussion.

The samples were prepared by casting from xylene solution, that is, from a three-component system. The resulting morphology may not be an equilibrium but instead a kinetically trapped mixture that reflects the processing history. However, as the samples were prepared identically, this does not mean that the concentration effect would be a metastable state seen only for one sample type.

We finally note that the molecular weight is expected to have an influence on the overall picture. Termonia et al.[36] have shown that for each molecular weight there exists a different temperature at which the draw ratio of PE reaches a maximum value. Elsewhere, Castro et al.[27] studied MEH-PPV blended with PS with the mixing ratio of 1:2 in spin-coated films and subsequently removed PS by a selective cyclohexane solvent. The AFM images revealed a smooth interface in the case of low and sharp spinodal decomposition in the case of high molecular weight PS. In the future, we expect to vary the molecular weight of the compounds as shown for pure PF2/6[32] and for MEH-PPV:PS blends[27] elsewhere.

## Conclusions

In summary, this study shows segregation and aligned microstructure of PF2/6 in tensile drawn PE blends. When the PF2/6 fraction is high (7−15 wt %), PF2/6 forms a mosaic of crystallites that are uniaxially aligned within PE crystallites. No evidence for macrophase separation is observed. In these samples, PF2/6 is well-aligned and the fwhm of the mosaic distribution of crystallites is ≤10°. When the PF2/6 fraction is low (0.25 wt %), PF2/6 takes a frozen-in nematic-like phase where molecules are aligned and some are still located close together. However, the coherence length is significantly a decreased as compared to the material with higher PF2/6 fraction. The reduced coherence length is interpreted as a decreased crystallite size. This behavior differs from that of BuEH-PPV,[17] which does not show crystallites but interstitial microfiber structure in well-aligned PE blend at high (30 wt %) BuEH-PPV fraction. This difference is attributed to the more rigid backbone of PF2/6 which is less entangled with the PE, meaning that when it is stretched the crystallites are not destroyed. These results give an insight for designing PF blends.

**Acknowledgment.** The XRD experiments were supported by the EC (RII3-CT-2004-506008 (IA-SFS)) and the XMaS project. R.C.E would like to thank FCT for a postdoctoral fellowship (SFRH/BPD/42450/2007). Thanks are moreover due to Wolfgang Caliebe of HASYLAB and Laurence Bouchenoire of the ESRF for assistance.

## References and Notes

(1) Winokur, M. J.; Chunwachirasiri, W. *J. Polym. Sci. B: Polym. Phys*. **2003**, *41*, 2630–2648.
(2) Scherf, U.; List, E. J. W. *Adv. Mater*. **2002**, *14*, 477–487.
(3) Knaapila, M.; Winokur, M. J. *Adv. Polym. Sci*. **2008**, *212*, 227–272.
(4) Scherf, U.; Gutacker, A.; Koenen, N. *Acc. Chem. Res*. **2008**, *41*, 1086–1097.
(5) O'Carroll, D.; Iacopino, D.; O'Riordan, A.; Lovera, P.; O'Connor, É.; O'Brien, G. A.; Redmond, G. *Adv. Mater*. **2008**, *20*, 42–48.
(6) Charas, A.; Ferreira, Q.; Farinhas, J.; Matos, M.; Alcácer, L.; Morgado, J. *Macromolecules* **2009**, *42*, 7903–7912.
(7) (a) Moons, E. *J. Phys.: Condens. Matter* **2002**, *14*, 12235–12260. (b) Veldman, D.; Meskers, S. C. J.; Janssen, R. A. J. *Adv. Funct. Mater*. **2009**, *19*, 1939–1948.
(8) Kulkarni, A. P.; Jenekhe, S. A. *Macromolecules* **2003**, *36*, 5285–5296.
(9) He, B.; Wu, C.; Huang, Y. *Macromol. Chem. Phys*. **2007**, *208*, 384–388.
(10) Biagioni, P.; Celebrano, M.; Zavelani-Rossi, M.; Polli, D.; Labardi, M.; Lanzani, G.; Cerullo, G.; Finazzi, M.; Duò, L. *Appl. Phys. Lett*. **2007**, *91*, 191118.
(11) Kuo, C.-C.; Lin, C.-H.; Chen, W.-C. *Macromolecules* **2007**, *40*, 6959–6966.
(12) Arias, A. C.; MacKenzie, J. D.; Stevenson, R.; Halls, J. J. M.; Inbasekaran, M.; Woo, E. P.; Richards, D.; Friend, R. H. *Macromolecules* **2001**, *34*, 6005–6013.
(13) (a) Cadby, A. J.; Dean, R.; Elliott, C.; Jones, R. A. L.; Fox, A. M.; Lidzey, D. G. *Adv. Mater*. **2007**, *19*, 107–111. (b) Morgado, J.; Moons, E.; Friend, R. H.; Cacialli, F. *Adv. Mater*. **2001**, *13*, 810–814. (c) Snaith, H. J.; Arias, A. C.; Morteani, A. C.; Silva, C.; Friend, R. H. *Nano Lett*. **2002**, *2*, 1353–1357.
(14) Cirpan, A.; Ding, L.; Karasz, F. E. *Polymer* **2005**, *46*, 811–817.
(15) Babel, A.; Li, D.; Xia, Y.; Jenekhe, S. A. *Macromolecules* **2005**, *38*, 4705–4711.
(16) King, S. M.; Vaughan, H. L.; Monkman, A. P. *Chem. Phys. Lett*. **2007**, *440*, 268–272.
(17) Yang, C. Y.; Heeger, A. J.; Cao, Y. *Polymer* **2000**, *41*, 4113–4118.
(18) Grell, M.; Knoll, W.; Lupo, D.; Meisel, A.; Miteva, T.; Neher, D.; Nothofer, H.-G.; Scherf, U.; Yasuda, A. *Adv. Mater*. **1999**, *11*, 671–675.
(19) Knaapila, M.; Stepanyan, R.; Lyons, B. P.; Torkkeli, M.; Monkman, A. P. *Adv. Funct. Mater*. **2006**, *16*, 599–609.
(20) Monkman, A. P.; Adams, P. *Synth. Met*. **1991**, *40*, 87–96.
(21) Weder, C.; Sarwa, C.; Bastiaansen, C.; Smith, P. *Adv. Mater*. **1997**, *9*, 1035–1039.
(22) Pålsson, L.-O.; Vaughan, H. L.; Monkman, A. P. *J. Chem. Phys*. **2006**, *125*, 164701.
(23) (a) Monkman, A. P.; Dailey, S.; Halim, M.; Horsburgh, L. E. *Synth. Met*. **1999**, *101*, 252. (b) Vaughan, H. L.; Monkman, A. P.; Pålsson, L.-O.; Nehls, B. S.; Farrell, T.; Scherf, U. *J. Chem. Phys*. **2008**, *128*, 044709.
(24) Heffelfinger, C. J.; Burton, R. L. *J. Polym. Sci*. **1960**, *47*, 289–306.
(25) Knaapila, M.; Hase, T. P. A.; Torkkeli, M.; Stepanyan, R.; Bouchenoire, L.; Cheun, H.-S.; Winokur, M. J.; Monkman, A. P. *Cryst. Growth Des*. **2007**, *7*, 1706–1711.
(26) Adhikari, R.; Godehardt, R.; Lebek, W.; Michler, G. H. *J. Appl. Polym. Sci*. **2007**, *103*, 1887–1893.
(27) Castro, F. A.; Graeff, C. F. O.; Heier, J.; Hany, R. *Polymer* **2007**, *48*, 2380–2386.
(28) Teetsov, J.; Vanden Bout, D. A. *Langmuir* **2002**, *18*, 897–903.
(29) Lieser, G.; Oda, M.; Miteva, T.; Meisel, A.; Nothofer, H.-G.; Scherf, U.; Neher, D. *Macromolecules* **2000**, *33*, 4490–4495.
(30) Knaapila, M.; Torkkeli, M.; Monkman, A. P. *Macromolecules* **2007**, *40*, 3610–3614.
(31) Lafrance, C.-P.; Pézolet, M.; Prud'homme, R. E. *Macromolecules* **1991**, *24*, 4948–4956.
(32) Knaapila, M.; Stepanyan, R.; Torkkeli, M.; Lyons, B. P.; Ikonen, T. P.; Almásy, L.; Foreman, J. P.; Serimaa, R.; Güntner, R.; Scherf, U.; Monkman, A. P. *Phys. Rev. E* **2005**, *71*, 041802.
(33) Monkman, A.; Rothe, C.; King, S.; Dias, F. *Adv. Polym. Sci*. **2008**, *212*, 187–225.
(34) (a) Holyst, R.; Schick, M. *J. Chem. Phys*. **1992**, *96*, 721–729. (b) Matsuyama, A.; Kato, T. *J. Chem. Phys*. **1996**, *105*, 1654–1660. (c) Subbotin, A.; Stepanyan, R.; Knaapila, M.; Ikkala, O.; ten Brinke, G. *Eur. Phys. J. E*. **2003**, *12*, 333–345.
(35) Grosberg, A. Y.; Khokhlov, A. R. *Statistical Physics of Macromolecules*; American Institute of Physics: Woodbury, NY, 1994.
(36) Termonia, Y.; Allen, S. R.; Smith, P. *Macromolecules* **1988**, *21*, 3485–3489.